SKI Report 97:35

Mechanism for the Effect of Sulphate on SCC in BWRs

July 1997

ISSN 1104-1374
ISRN SKI-R--97/35--SE

SKI
STATENS KÄRNKRAFTINSPEKTION
Swedish Nuclear Power Inspectorate

SKI Perspective

Stress corrosion cracking is one of the most serious materials related problems encountered in BWRs. The crack propagation rate has been shown to be strongly affected by sulphates in the coolant. Typical concentrations of sulphates and other anions in the primary water is 1 ppb. The values can increase temporarily to much higher values during transients. Shorter periods of such extra exposure give no effect, but there seems to be an integrated threshold value ("memory effect") beyond which the propagation rate increases rapidly, as reported by Per Lidar in work sponsored by SKI and the Swedish utilities, and published in the Proceedings of the Seventh International Symposium "Environmental Degradation of Materials in Nuclear Power Systems - Water Reactors", Breckenridge, Colorado, August, 1995

SKI therefore approached Studsvik Material AB to bring together chemists and materials experts in an attempt to develop an hypothesis for the behaviour of sulphate and to explain why sulphates are the most aggressive of ions. Part 1 of this report is the result of that initiative. It considers only the propagation phase and does not attempt to discuss any aspects of crack initiation or the known effects of other ions, such as chlorides, on SCC since the original work only used sulphates and indicted that there could a memory effect associated with sulphates.

The report has also been presented, and published in the Proceedings of the eighth International Symposium "Environmental Degradation of Materials in Nuclear Power Systems - Water Reactors", Amelia Island, Florida, August, 1997. Before this the original report was printed in Swedish: SKI Report 96:79.

The hypothesis is that the rate determining step of the crack propagation should be found in the set of processes on the cathode like adsorption, transportation, chemical transformation and precipitation in which hydrogen sulphate and sulphate participate while migrating through the cathodic area towards the crack. It is also postulated that the permeability and geometry of the cathodic surface oxide will be influenced by sulphate and other sulphur containing species breaking down the passive film.

Sulphate entering the crack environment can be reduced down to sulphide or other sulphur compounds that form deposits together with metal ions formed in the anode process. Deposits are believed to alter the oxide in the cathodic areas and to contribute to the permeability of this oxide as well as to the growth and extension of the cathodic area. The acid function of hydrogen sulphate could also neutralise hydroxide ions formed in the cathodic process.

Both the sulphate induced growth of the cathodic area and the acid function of hydrogen sulphate could explain the increased crack growth rate and the observed memory effect.

In order to try and find out if there was a firm basis for the hypothesis SKI approached AEA Technology in Harwell to examine a specimen from the original work of Per Lidar. The report of this work is printed in Part 2 of this report. It was also presented at the Eighth International Symposium "Environmental Degradation of Materials in Nuclear Power Systems - Water Reactors", Amelia Island, August, 1997, but was not included in the written publication.

The results support the hypothesis, but are not conclusive as to the exact chemical processes involved. For this more detailed studies of the crack surfaces are needed using sample preparation techniques that are under development.

SKI considers that there is still need for work to explain and predict the effect of different impurities on the crack propagation rates of stress corrosion crack propagation. This is true both for large deviations from normal conditions, but also for the low concentrations which persist during normal operational conditions. Their accumulative effects must be explained for the purposes of predicting crack propagation rates and the risk for initiation of stress corrosion cracks in BWR plants.

Karen Gott
Department of Structural Integrity
SKI Project Manager

SKI Report 97:35

Mechanism for the Effect of Sulphate on SCC in BWRs

Part 1: Hypothesis

Hans-Peter Hermansson [1]
Karen Gott [2]

[1] Studsvik Material AB, SE-611 82 Nyköping, Sweden
[2] Swedish Nuclear Power Inspectorate,
SE-106 58 Stockholm, Sweden

July 1997

SKI Project Number 96082

Table of Contents

Summary

Stress corrosion cracking is one of the most serious materials related problems encountered in BWRs. The crack propagation rate has been shown to be strongly affected by sulphates in the coolant. Typical concentrations of sulphates and other anions in the primary water is 1 ppb. The values can increase temporarily to much higher values during transients. Shorter periods of such extra exposure give no effect, but there seems to be an integrated threshold value ("memory effect") beyond which the propagation rate increases rapidly, as reported by Per Lidar at the seventh International Symposium "Environmental Degradation of Materials in Nuclear Power Systems - Water Reactors", Breckenridge, Colorado, August, 1995.

The primary system surfaces communicating with the bulk water are normally protected by a very thin, passivating oxide film. This is composed of spinel phases like chromite, situated closest to the metal upon which there could be a layer of nickel ferrite. On top of the spinels there is also normally a cover of deposits. This composite film is going to act as a surface for adsorption, transportation and storage of sulphates from the primary bulk water.

Starting from a comparison of the surface conditions around a corrosion pit it was proposed that in the close vicinity of an active crack, the surface oxide is going to function as a cathode on which pH and also the potential are high compared to the surrounding surfaces. The permeability of the oxide is essential for the cathodic function as chemical species and charge have to be transported through it.

This has led to the hypothesis that the rate determining step of the crack propagation should be found in the set of processes on the cathode like adsorption, transportation, chemical transformation and precipitation in which hydrogen sulphate and sulphate participate while migrating through the cathodic area towards the crack. It is also postulated that the permeability and geometry of the cathodic surface oxide will be influenced by sulphate and other sulphur containing species breaking down the passive film.

Sulphate entering the crack environment can be reduced down to sulphide. Intermediates like polysulphides (disulphide and others) and also thiosulphate might be formed. Intermediates and sulphates themselves can form deposits together with metal ions formed in the anode process. Deposits are believed to alter the oxide in the cathodic areas and to contribute to the permeability of this oxide as well as to the growth and extension of the cathodic area. The acid function of hydrogen sulphate could also neutralise hydroxide ions formed in the cathodic process.

Both the sulphate induced growth of the cathodic area and the acid function of hydrogen sulphate could explain the increased crack growth rate and the observed memory effect.

Introduction

IGSCC is one of the major material problems in BWRs, and an understanding of crack propagation under different conditions is an important factor when assessing the structural integrity of nuclear components. From the regulatory point of view it is important to be able to assess the effect of transients on crack propagation rates, including chemical transients which raise the conductivity above action levels. The Swedish Nuclear Power Inspectorate (SKI) has studied various aspects of crack propagation for many years. One area of great interest in this respect is how cracks react to transients and SKI together with the Swedish utilities has sponsored the study of some chemical transients in recent years [1, 2]. The results of the sulphate transient studies on stainless steel showed that short periods with high sulphate concentrations have no effect, but repeated periods increase the crack propagation rate [1]. No explanation for this was proffered in the earlier work.

SKI therefore approached Studsvik Material AB to bring together chemists and materials experts in an attempt to develop an hypothesis for the behaviour of sulphate and to explain why sulphates are the most aggressive of ions. This paper is the result of that initiative. It considers only the propagation phase and does not attempt to discuss any aspects of crack initiation or the known effects of other ions, such as chlorides, on SCC since the original work only used sulphates and indicted that there could a memory effect associated with sulphates.

The work was started with a literature study in which literature on crack propagation was specifically excluded (since this was part of the earlier work) and the search was concentrated to sulphate, sulphate pick up, diffusion, adsorption, oxides and oxide morphology. The results were not very numerous. However the literature clearly showed a connection between sulphate concentration and crack propagation rates including a number of implications concerning a memory effect [1, 3]. Memory is defined as a number of exposures being needed before sulphate affects the crack propagation rate, and that the rate increases with the number of exposures. A clear connection was also found between the effect of thiosulphate and an increase in the crack propagation rate [3, 4, 5]. The literature also provided support for the premise that the area in and around the crack opening is cathodic [6].

Water phase

In the bulk phase outside the passive film there are low concentrations (about 1 ppm) of anions such as chloride, nitrate and sulphate under normal conditions. During chemical transients these concentrations can temporarily increase by several orders of magnitude, which has consequences for amongst other things their uptake on surfaces in contact with the bulk water.

For the continued discussion it is important to realise how these different chemical systems act. The sulphate system exists for example mostly as hydrogen sulphate, HSO_4^- in bulk water at 285 °C and only a small amount of the total concentration exists as sulphate, SO_4^{2-}, see Figure 1 [7, 8]. Chloride, Cl^-, and nitrate, NO_3^-, have no variants.

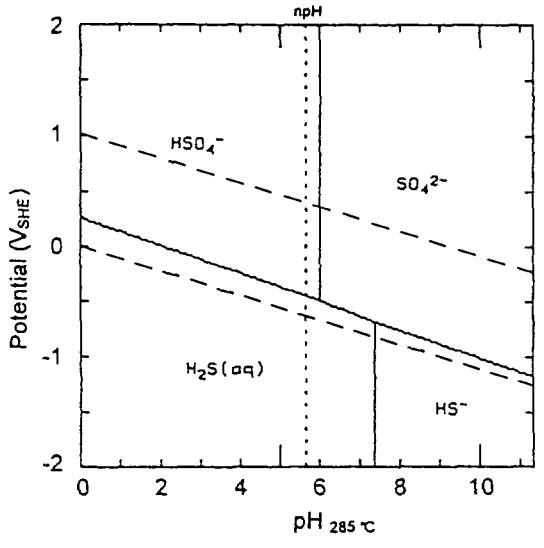

Figure 1: *Pourbaix diagram for sulphate at 285 C. [8]*

Oxide phase

Figure 2 illustrates, in a much simplified manner, the build up of the passive film on stainless steel in the primary system of a BWR with normal water chemistry without hydrogen additions, showing the regions of importance for the adsorption and transport processes. Theoretical discussions and practical experience imply that the film probably consists of two or more distinguishable layers comprised of spinel phases which have grown in situ, as well as an outer layer of deposit. A more detailed description can be found in amongst other references [9, 10].

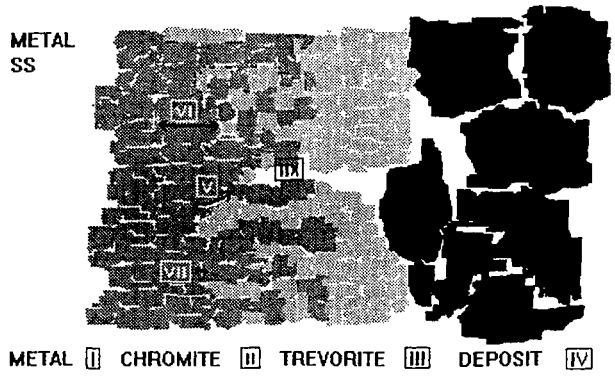

Figure 2: *Simplified illustration of the build up of the oxide film on stainless steel at 288 C under NWC conditions.*

Legend: Regions of importance are indicated by Roman numerals

I	Transition metal/chromite *dark grey*
II	Transition zone chromite/trevorite *light grey*
III	Transition zone trevorite/deposit *black*
IV	Transition zone deposit (surface effects)/liquid
V	Longitudinal grain boundary diffusion
VI	Trancrystalline transport processes
VII	Transversal grain or layer transport
VIII	Transport in pores (including liquid)

There is a difference between the formation of the passive film which forms on a steel surface during the relatively short autoclave exposure and that in a primary system of a BWR which is built up over many years. The discussion which follows only considers the passive film on a stainless steel surface in a BWR with NWC. The inner layer in such a film can be expected to consist of the spinel "chromite", $FeCr_2O_4$, or of chromium oxide, Cr_2O_3, and the outer layer of the spinel "trevorite" $Ni_xFe_{3-x}O_4$, $0 \leq x \geq 1$. Trevorite can also have a range of compositions, ie "x" can vary between the different

trevorite crystals in the layer. The interface between the inner and outer layers is not sharp, but is assumed to comprise of a zone in which the two spinel phases coexist in separate on phase crystals.

Experience shows that the thickness of the film can vary within wide ranges, from tens of nanometres to a few micrometers. In particular the trevorite layer can also be riddled with cracks, pores and other defects which means that there is a chemically active surface area which is larger than the geometrical. Further a volume is offered, where the impurities can remain before they precipitate, are stored or incorporated by modification processes.

In reality the film, and principally the trevorite layer, will be more or less contaminated by other elements than the main components of stainless steel. The impurities can be enriched in for example the grain boundaries and locally reach relatively high concentrations. Thus they can also have a considerable effect on the transport processes. The chromite phase is in contrast relatively clean.

The deviations from perfection described will not only affect the ion and vacancy transport but also the electron behaviour. A severely contaminated grain boundary or a transformed crystallite will have a different electron conductivity than neighbouring crystallites. For example intrusions of other phases, such as sulphides and or sulphates can be expected to affect the electric conductivity and passivation capacity considerably. The effect of impurities on the conductivity of the film is important, but difficult to quantify.

The film can react as a semi-conductor and will act as a cathode in the vicinity of an active crack. In the film a special chemical micro-environment will exist determined by the condition of the films, the dominant physical and chemical parameters of the system and whether or not the area in the immediate vicinity of the crack is cathodic.

The corresponding film produced during laboratory exposure is much simpler, not often comprised of the different oxide layers and consequently also typically much thinner.

In Figure 3 the variation in potential relative to a normal hydrogen electrode is indicated from the bulk water down to the crack tip. Since NWC is assumed the potential in the bulk water is taken to be 0 to 100 mV. Bulk water is normally slightly acidic because of the hydrolysis of metal ions released by the corrosion processes. This means that the system surfaces generally will have a weak positive ζ–potential of the order of a few tens of mV relative to the bulk water. The surface potential will thus lie in the region of 20 to 120 mV on surfaces outside the cathodic region. Because of the gradient and other factors including those of an hydrodynamic character, the bulk water anions will wander to the surface and to some extent be adsorbed there.

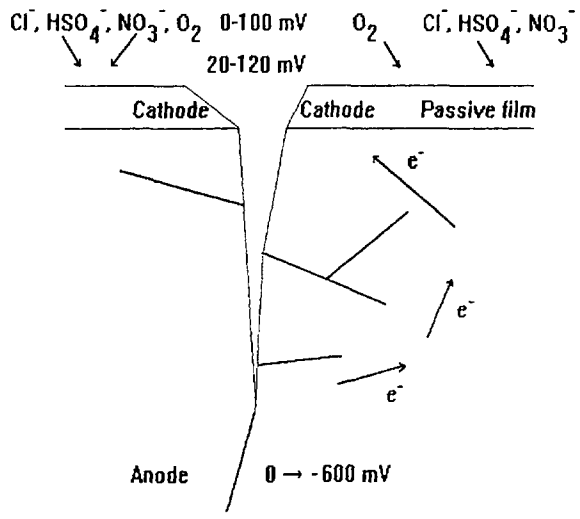

Figure 3: *Schematic sketch of a crack with the surrounding potentials at various points relative to a normal hydrogen electrode*

Since the cathode surface in the close vicinity of the crack has a higher potential, adsorption will occur more quickly there than on the larger system surfaces outside the cathodic areas. It is probable that similarly charged ions such as Cl^-, HSO_4^- and NO_3^- will behave similarly in this primary adsorption process. SO_4^{2-} can be expected to be more strongly adsorbed than the others because of its charge is twice as large and has a greater polarisablilty. SO_4^{2-} has a much lower concentration than HSO_4^- in the slightly acidic bulk water, but will be the dominant of the two on the cathode surface because of the slightly higher pH which exists there.

Transportation on the oxide surface

The surface in the vicinity of the crack is cathodic. This means that the pH there will be relatively high because of the local formation of hydroxyl ions as a result of the cathodic reaction:

$$O_2 + 2H_2O + 4e^- = 4OH^-$$

The potential in the cathode region can be expected to be higher than the potential for the surrounding surfaces which are not cathodic this has been demonstrated by sweeping over pits with micro electrodes [6, 11]. This means that the ions have a greater driving force to deposit from the bulk water on the cathodic region, but also that the anions

which are adsorbed outside the cathodic region will migrate towards this and the crack opening.

The pH increases when the anions migrate to the increasingly cathodic region. This has no particular effect on Cl^- and NO_3^-. On the other hand HSO_4^- will transform to SO_4^{2-} in the cathodic region according to the reaction:

$$HSO_4^- + OH^- = SO_4^{2-} + H_2O$$

The sulphate ion can then, because of its greater polarisability, be expected to be more strongly retained than the chloride and nitrate in the cathodic area, even after the sulphate concentrations have decreased in the bulk water after a transient. Sulphate can be retained as such in the adsorbed form or in the form of a precipitated reaction product. With repeated sulphate transients there will therefore be an increasing amount of sulphate transported to the cathodic region, and to a greater extent retained there by the various processes.

That chloride and nitrate do not behave in the same manner as sulphate can be explained by the fact that these ions can more easily be washed out after the transient has subsided. This is probably also true for hydrogen sulphate which settles on surfaces outside the cathodic areas, and this might also explain why sulphate cannot be detected to any great extent on surfaces outside the cathodic regions in the system.

Electrochemistry of the crack

A summary of the processes in the crack and its immediate vicinity is presented in Figure 4, which differs from Figure 3 in that the concept of a possible anode and cathode is introduced. Further examples are included of solid sulphur containing species, which could be incorporated in the cathode region resulting in a continuous alteration to its properties. In the discussion the behaviour of iron is used as a model, but other metals in the stainless steel (such as nickel and chromium) of course also change in accordance with their specific chemistries. The main processes are the anode reaction at the crack tip, where the iron (and other metals) are dissolved and form iron (II) ions and electrons, as well as the cathodic reaction in the crack opening and on the surfaces immediately outside the crack, where in the first hand oxygen is reduced to hydroxide. Iron (II) ions are hydrolysed which results in the anodic environment at the crack tip becoming acidic. The electrochemical processes are maintained by these reactions as well as the transport processes in which electrons, iron and other species migrate out of the crack, and ions which have their origin in the bulk water migrate into the crack meeting the iron species.

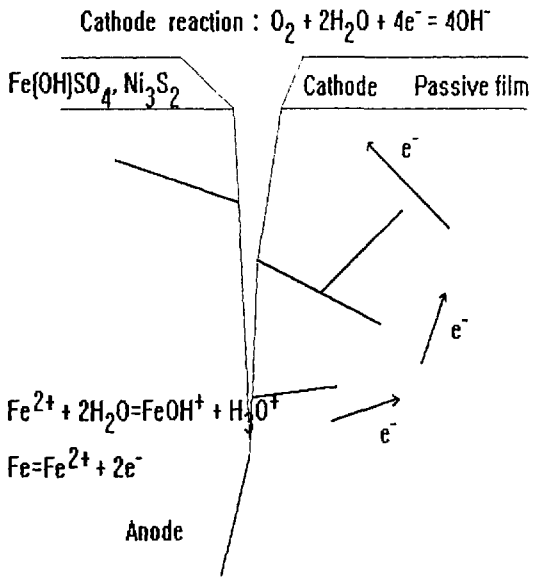

Figure 4: *Summary of some details of the crack environment*

The rate determining step for the crack propagation can be found in these transport processes as well as in how easily, to what extent and at what speed the electrode reactions can occur. The cathode surface geometry and size, as well as its chemical environment are also important factors.

Apart from the anodic reaction of iron with the subsequent hydrolysis step, see Figure 4, a number of different processes can occur in the anodic crack tip region which is characterized by a low pH and low potential. The different metals in the steel (Fe, Cr, Ni) and the supply of sulphur containing species can participate in several ways.

Examples of some reactions and reaction products which can occur in a crack depending on the potential and other conditions are listed below in no special order to further illustrate the concept presented in Figure 4:

$Fe^{2+} + SO_4^{2-} = FeSO_4(s)$
$8e^- + 5H_2O + SO_4^{2-} = HS^- + 9OH^-$
$5H_2O + 2SO_4^{2-} + 8e^- = S_2O_3^{2-} + 10OH^-$
$Fe^{2+} + S_2^{2-} = FeS_2(s)$
$2HS^- + 2OH^- = S_2^{2-} + 2H_2O + 2e^-$
$HS^- + H_3O^+ = H_2S + H_2O$
$Ni(s) = Ni^{2+} + 2e^-$
$Cr(s) = Cr^{2+} + 2e^-$.

Examples of reactions and reaction products which can occur in the outer cathodic region of a crack are listed below in no special order:

$$3Ni^{2+} + 2S^{2-} = Ni_3S_2(s)$$
$$Fe^{3+} + OH^- + SO_4^{2-} = Fe(OH)SO_4(s).$$

Figure 4 also provides a general picture of crack propagation. In the anodic area at the crack tip metal is dissolved, symbolized by the formula for iron dissolution.

In a propagation situation the cathodic surface will lie partly outside the passive film, see amongst other [6, 11]. In the presence of oxygen, even low concentrations, the cathode reaction will use electrons and build hydroxyl ions, OH^-.The pH will therefore be relatively high in those parts of the passive film which lie within the cathodic region. This can contribute to the oxide in the cathodic region, in particular chromite, becoming unstable if the pH becomes too high.

With access to less oxygen there is a possibility of forming hydrogen in the cathodic reaction, providing the driving for of the anodic reaction is sufficient for such as situation to develop. This could occur if the metal ions formed at the crack tip have a very low chemical activity, for example because of complex formation or precipitation reactions. The pH will still be relatively high on the cathodic surfaces even in this case because of the reaction:

$$2H_2O + 2e^- = H_2 + 2OH^-.$$

Transportation within the crack

The stability of the passive film will be affected by the increased pH existing in the cathode region. All simple oxide phases, but also spinels become destabilised at both low and high pH. This means that the oxides in the cathode region will dissolve or at least begin to transform if the pH is increased sufficiently. The rate for this process is difficult to predict. Experience in the laboratory at the appropriate temperatures show however that chromite dissolves so fast that the process can be clearly detected after only short exposures, of the order of a couple of weeks.

Because of the greatly increased concentration of metal ions, for example Fe^{2+}, in the active crack tip, the pH will decrease there as a result of hydrolysis. The hydrolysis complexes thus formed will migrate outwards in the chemical gradient, and anions will migrate inwards into the crack. Since the potential falls in the crack, secondary reactions such as reduction will occur, which is illustrated in Figure 4 and the pertaining list of

possible reactions. Further precipitation can occur because of local very high concentrations of chemical components. Examples of reactions inside the crack are of the following types:

- Anodic formation of amongst other things Fe^{2+}, Ni^{2+}, at the crack tip.

- Hydrolysis of anodically formed metal ions, for example of Fe^{2+}. This leads to acidification of the crack tip environment, which contributes to maintaining the attack, since amongst other things no new passive film can be formed in the acidic environment.

- Formation of complexes between the anions migrating inwards and the metal ions and their primary hydrolysis complexes migrating outwards, for example the $FeCl_n^{-(n-3)}$ complex.

- Precipitation of sulphates, for example iron sulphate. Other possible sulphates are those of nickel and chromium.

- In the strongly reducing environment sulphate can be reduced to sulphide, disulphide, thiosulphate and other sulphur containing species with lower oxidation states than sulphate. Such reactions have been verified [3, 4, 5]. The above mentioned metal complexes can in turn react, for example iron with disulphide to form iron sulphide, FeS_2. Nickel can form Ni_2S_3 at the temperatures of interest [7]. The sulphur containing phase can precipitate and deposit in the crack environment, or in the cathodic region at and near the mouth of the crack.

- In the acidic environment at the crack tip H_2S can be formed and escape or participate in sulphide precipitation.

The sulphate and sulphide phases formed work partly as storage media for sulphur, to the extent that they deposit in the crack, or in the and on the oxide at the mouth of the crack and its immediate vicinity in the cathodic region. They will also affect the cathodic oxide integrity and, probably in combination with the effects of a pH increase, reduce its passivating capability by gradual dissolving of the chromite. This kind of sulphur deposit in the form of iron sulphide has been observed in the oxide around pits [12]. Thiosulphate, $S_2O_3^{2-}$, has also been found to have a strong effect on crack propagation [3, 4, 5].

Crack chemistry hypothesis

Since the literature search gave a relatively meagre result, but anyway some important indications, the work was directed to in some detail try to propose hypotheses concerning the sulphate chemistry in the different parts of the crack. This applies in particular to its nearest surrounding of the passive film surface. As described above the work was directed to finding parameters which are important for this dynamic development and in particular the role of repeated, temporarily high sulphate concentrations in the bulk water can have for crack propagation. There is special value if some definitive part of the mechanism postulated can be tested by a simple experiment. A number of the processes implied in Figures 3 and 4 reflect the importance of sulphate for the propagation rate.

The previous discussion can be summarized in the following hypothesis:

1. The cathode reaction is favoured by hydrogen sulphate adsorption and transport to the cathode, where hydroxide will be consumed because of the acidic role of the hydrogen sulphate.

2. The cathode region will successively extend itself with each transient through degradation of the oxide amongst other things because of the increase in pH and that the alkaline iron sulphate, iron sulphide and nickel sulphide precipitate on the cathode surface and in its periphery.

3. The cathode expansion and retention of sulphur species is the cause of the memory effect observed and the increase in the stress corrosion cracking propagation rate associated with sulphate transients.

In order to test this hypothesis as a first step the sample originally used to determine the effect of sulphate transients on the crack propagation rates in stainless steel will be analysed using SIMS and Laser Raman Spectroscopy to try and detect the occurrence of the sulphur bearing species, and to study the degradation of the oxide layer in the cathodic region [1].

Further possible ways to test these hypotheses include high temperature measurements of the pH using a microelectrode and hopefully observing a pH increase of the cathode region associated with sulphate additions. The second point can be tested by micro potential measurements of the cathode region. At a later stage calculations using for example the model of Chun takes into account the latest information and describes different processes which he considers can occur in a crack, amongst other things with respect to the kinetics to assess the sensitivity of different parameters could also be performed [13].

Acknowledgements

The Swedish Nuclear Power Inspectorate has financed this work which has been greatly enhanced by discussions with Per Lidar and Sture Eriksson, Studsvik Material AB. The authors thank them for this help.

References

1 Lidar, P., *Influence of sulfate transients on crack growth in type 304 stainless steel in water at 288°C*, Proc. seventh Int Symp Environmental Degradation of Materials in Nuclear Power Systems - Water Reactors, Breckenridge, Colorado, August, 1995, p. 597-608, NACE International, Houston, Texas (1995)

2 Lidar, P., *Environmental enhancement of crack growth in type 304 stainless steel in water at 288°C*, Proc. International Symposium on Plant Aging & Life Prediction of Corrodible Structures, Sapporo, Japan, May, 1995, Japan Society of Corrosion Engineering, Tokyo, Japan, (1995).

3 Staehle, R., *Private communication*, October 1996

4 Ljungberg, L. G., et al, *Effects of impurities on IGSCC of stainless steel in high temperature water,* Corrosion 87, San Francisco, California, March, 1987, paper 87, NACE, Houston, Texas, (1987).

5 Ljungberg, L. G., et al, *The effect of sulfate on environmental cracking in BWRs under constant load or fatigue*, Corrosion 89, New Orleans, Louisiana, April, 1989, paper 617, NACE, Houston, Texas, (1989).

6 Bates, S. J., et al, *Design and development of scanning reference electrode technique for investigation of pitting corrosion in FV 448 gas turbine disc steel,* Materials Science and Technology, **5**, 356-361 (1989).

7 Beverskog, B., *Private communication*, October 1996.

8 Beverskog, B., *Pourbaix diagram för systemet Fe-Cr-Ni-S vid 25 - 300°C*, (In Swedish), Internal report, Studsvik Material AB, Nyköping, Sweden (1996).

9 Hermansson, H-P., et al, *Kinetik i oxidskikt*, (In Swedish), ABB report: KEMOX R-012, April 1995, Atom AB/Studsvik Material AB, Sweden (1995).

10 Hermansson, H-P., et al, *Kinetics in passivating oxide films*, Water Chemistry of Nuclear Reactor Systems, BNES 7, Bournemouth, UK, October, 1996, British Nucelar Energy Society, London, UK, (1996).

11 Sargeant, D.A., et al, *Microcomputer controlled scanning reference electrode technique apparatus developed to study pitting corrosion of gas turbine disc steel,* Materials Science and Technology, **5**, 487-491 (1989).

12 Ashmore, C. B., et al, *Water side corrosion of ferritic steel steam generator tubing under acid sulphate-chloride conditions*, British Corrosion J, **24(2)**, 113-125 (1989).

13 Chun, J. H., *Modelling of chemistry related to environmentally assisted cracking in low-alloyed steels*, D Sc Thesis, MIT, February 1995.

SKI Report 97:35

Mechanism for the Effect of Sulphate on SCC in BWRs

Part 2: Microstructural Examination of an Oxide Layer on Steel

Ian Vatter, Alison Crossley and Gina Cattle

AEA Technology, 220 Harwell, Didcot,
Oxfordshire, OX11 0RA, United Kingdom

July 1997

SKI Project Number 97129

Contents

Executive Summary

Analysis of the composition of the oxide present within the IGSCC region on a fractured CT specimen which had been tested in simulated BWR coolant with transient additions of sulphate has been carried out. The techniques employed were scanning electron microscopy with energy dispersive x-ray detection(SEM-EDX), Laser Raman Microprobe Spectroscopy (LRM) and Secondary Ion Mass Spectrometry (SIMS). Each technique was able to detect the presence of a duplex oxide film on the surface of the sample and also in cracks penetrating the sample. The oxide layer adjacent to the metal was chromium rich and the other layer was rich in iron. The size of the features were on the limit of the spatial resolution of the LRM technique. The SEM was the only technique to detect the presence of sulphur associated with the iron rich oxide within a crack. No sulphur was detected in either type of oxide on the surface of the sample.

Introduction

Stress corrosion is a problem encountered in BWR materials. The crack propagation rate has been shown to be strongly affected by the presence of sulphates in the coolant. The aim of this programme was to investigate the oxide layer present on the surface and within cracks on a CT sample which had been tested in simulated BWR coolant water with transient additions of sulphates. The samples were pre-fatigued, then subjected to conditions to produce intergranular stress corrosion cracking (IGSCC). Finally the samples were subjected to a post fatigue to fracture the sample.

The programme involved the use of scanning electron microscopy (SEM), laser raman microprobe (LRM) spectroscopy and secondary ion mass spectroscopy (SIMS) to identify the region of IGSCC and subsequently to analyse the chemical composition of the oxide, with particular interest in the sulphur content of the oxide films.

Sample Preparation

After receipt of the CT sample (165-21) it was examined using a scanning electron microscope (SEM) to determine the various fracture modes present on the surface and locate the region of IGSCC. Figure 1 shows an SEM image of the IGSCC region. This permitted the correct area for examination by further analytical techniques to be selected.

After examination by SEM the sample was sectioned to give a sample of approximate dimensions 6x3x3mm. This section contained both intergranular and transgranular regions of fracture. The section was mounted transversely in epoxy resin and the surface polished to a 1 μm finish. The sample was then examined using an optical microscope to check the surface finish and confirm that the surface oxide had been retained.

Scanning Electron Microscopy (SEM)

After preparation of the sample it was returned to the Leica S440 SEM for examination. The aim of using the SEM was to select a region of the sample for subsequent analysis by Raman Spectroscopy and secondary ion mass spectrometry (SIMS) and also to gain chemical composition data using the energy dispersive x-ray (EDX) detector. The EDX detector interfaced to the S440 SEM is configured to enable detection of elements of Z=6 and above. Thus it is possible to identify oxide layers.

From the image in the SEM it was possible to locate the region of intergranular fracture and using the EDX detector the presence of oxide on the surface of the sample was confirmed. It was also noted that within the region exhibiting intergranular cracking there were cracks penetrating the sample, these cracks appeared to be following grain boundaries and some were found to be filled with oxide.

The chemical composition of a selection of precipitates within the matrix of the sample was checked and found to consist of manganese sulphide, nickel sulphide, calcium aluminosilicate occasionally with titanium. Precipitates of nickel sulphide were also found within cracks. The oxide layer on the surface of the sample was approximately 5-10 μm in thickness and the cracks penetrating the sample were approximately 3 μm in width. The oxide had a duplex appearance in the SEM backscattered electron image (e.g. figure 2) and analysis using the EDX detector confirmed that the chemical composition of the oxide layer changed between the inner layer adjacent to the metal and the outer layer. The inner layer was richer in chromium and the outer layer was depleted in chromium, the latter consisting predominantly of iron oxide. The inner oxide

layer was also thinner than the outer layer. The area of investigation was situated close to the onset of the IGSCC. The variation of chemical composition across the oxide layer was further investigated by collecting EDX Linescans. The elements measured were oxygen, aluminium, silicon, sulphur, calcium, titanium, chromium, manganese, iron and nickel as these were the elements found to be present in the matrix and precipitates. Linescans were collected transverse to an oxide filled crack, along an oxide filled crack and also across the oxide layer on the surface of the sample. The linescans and associated images showing locations are shown in figures 2-8. The linescan traces for aluminium, silicon calcium and titanium have not been included as they did not show any features of interest. The linescans across the oxide within a crack (figures 4 and 5) showed the differences in the oxide composition, with iron being depleted adjacent to the metal and chromium and nickel being depleted from the oxide in the centre of the crack. At portions of the linescans evidence can be seen of both manganese sulphide precipitates in the matrix and nickel sulphides within the oxide layer. As the crack got narrower the evidence of a duplex oxide disappeared (figure 6). In addition there was evidence that the iron rich central region of the oxide layer was enriched with sulphur. Similar linescans taken across the oxide layer at the surface (figures 7 and 8) of the sample showed similar features with the exception of the sulphur enrichment which was not observed.

Laser Raman Microprobe Spectroscopy

After analysis in the SEM the sample was transferred for analysis using laser Raman microprobe spectroscopy. The objective of this analysis was to identify the corrosion products (chemical phases) and determine their spatial distribution. We were particularly interested in presence of sulphate compounds.

The size of most of the features of interest was on the limit of spatial resolution of the laser Raman microprobe. Iron spinel (Fe_3O_4) is the main corrosion phase present within the crack and on the sample surface. However, there are localised areas of spinel material which is deficient in iron, for example within the duplex scale. No sulphate or chromia was detected.

The crack within the intergranular region characterised in the SEM was relocated and was examined in detail, as shown in figure 9 :

A crack further into the intragranular region was also examined by laser Raman microprobe spectroscopy (figure 10).

Raman spectroscopy is an optical technique whereby chemical and phase specific information can be obtained non-destructively with a spatial resolution of 2 - 4 μm. The laser Raman microscope is based around a Spex Triplemate Spectrometer, fitted with a liquid nitrogen cooled CCD detector and Nikon microscope. Spectra were recorded in the back-scattered geometry, using a x 40 high numerical aperture objective lens. The

backscattered light was filtered through a pin hole aperture to give a spatial resolution of approximately 2 μm. The exciting laser wavelength was 514.5 nm (from an air cooled Ar^+ ion laser). The power was approximately 100 mW. The wavelength scale was calibrated against the emission lines of a neon lamp. A schematic of the experimental arrangement is shown in figure 11.

The laser is sent through a series of optical elements which define the polarisation and direction of the laser beam. This passes through a beam splitter, which sends the laser beam down the microscope. It emerges through an objective lens and illuminates the sample surface at a specific spot. The 180 degree backscattered light is then collect by the same objective lens and the beam passed up the body of the microscope through the beam splitter where it is re-directed into the spectrometer. The elastically scattered light (i.e. light of the same frequency as the incident laser beam (514 nm) is filtered out and the remaining inelastically scattered light (i.e. light which has undergone a frequency change by interaction with the sample) is dispersed over a detector (the spectral band pass of our system is set at approx. 20 nm). The Raman spectrum is generated by phonon interactions of the crystal structure with the light beam. Thus the Raman spectrum is characteristic of both chemical composition and crystal phase of a particular material.

There are inhomogeneities clearly visible in the optical and scanning electron micrographs of the crack. However, most of these features are at or beyond the spatial resolution of the laser Raman microprobe. For example a duplex scale is clearly visible in the SEM image but it was not possible to differentiate the two layers optically.

Crack A

Analysis point A1, A2

This was a brighter "inclusion" at an elbow point approximately 20 microns from the surface. The spectra were commensurate with an iron rich spinel phase, eg. Fe_3O_4 or a transition metal substituted spinel $T_xFe_{3-x}O_4$, where T = Mn, Cr, etc.

Analysis point A3, A4

An attempt was made to differentiate the two layers of the duplex scale. A4 was a point actually the exposed outer surface of the sample, where incomplete encapsulation of the mounting media had occurred. Spectrum 3 is very similar to those obtained from A1 and A2. However in spectrum 4 the spinel band (broad band centred around 700 cm^{-1}) has moved to lower wavenumbers and the Fe-O bands at approximately 220 and 280 cm^{-1} have disappeared. This spectrum is indicative of a mixed phase spinel possibly poor in iron, eg. $Mn_{1.5}Cr_{1.5}O_4$. Note that point 4 may actually be an area where the outer scale surface has been removed during

	sample preparation and we may be probing the inner duplex scale.
Analysis point A5, A6	The spectra obtained at these points, deep within the corrosion crack are similar to those obtained at A1, A2 and A3, indicating the presence of an iron rich spinel phase, eg. Fe_3O_4.
Analysis point B1	Little was discernible from the spectra obtained at this point. It would appear that this was dominated by either the mounting media or even large void fractions, possibly arising from pull out during sample preparation.
Analysis point B2, B3	This was a bright inclusion present in the crack. No spinel band was present. However a band at approximately 260 cm^{-1} was observed on a Rayleigh background (this arises from the reflective surface). This band was not due to scattering from any of the reference materials. We can theorise that it may be due to a defective sulphide (Mn) inclusion.
Analysis point B4	The iron rich spinel band is observed in spectra obtained from this point. However the signal is weak and no Fe-O bands were observed.

At no point was the any evidence for the presence of sulphate. The sulphate group is a relatively strong Raman scatterer with an intense and very sharp band at approximately 980 cm^{-1}. We also did not detect the presence of chromia (Cr_2O_3) which again is a strong Raman scatterer with an intense band at approximately 560 cm^{-1}.

Secondary Ion Mass Spectroscopy (SIMS)

After examination of the sample by the techniques of SEM-EDX and Raman spectroscopy the sample was transferred into a Vacuum Generators MA500 Secondary Ion Mass Spectrometer for further analysis.

The MA500 is equipped with a gallium primary ion source operated at an accelerating voltage of 25 keV and a beam current of approximately 1 nA. This produces a primary ion beam with high current density which can be focused down to a minimum spot size of 50nm. The sample is imaged using the ion induced secondary electron signal. The secondary ions emitted by the sample are collected by a quadrapole mass spectrometer to allow elemental analysis. The same region of the sample as previously examined in the SEM and LRM was located and analysis was carried out on the secondary ions emitted by the sample. The elements for which analysis was attempted were iron, chromium, nickel, oxygen and sulphur.

Figure 12 shows the ion induced secondary image, the chromium ion image and the iron ion image collected from the region of interest. Note that the image produced by the SIMS is the mirror image of that produced by the SEM and LRM. The oxide in the crack shows up brighter than the adjacent matrix in both the chromium and iron images due to the increased secondary ion yield which is produced from an oxide. It can be seen from this set of images that the extent of chromium rich oxide is greater than the iron rich oxide within the crack confirming the findings of the SEM of a duplex oxide with the layer adjacent to the metal being chromium rich. At the sample surface the iron signal is more extensive than the chromium as the iron rich oxide sits on the outer surface which is again consistent with the findings of the SEM analysis. As with the investigation using the LRM no indication of sulphur was found within either the oxide layer on the surface of the sample or the oxide within the crack.

Summary

- The CT sample supplied by Ski was examined and the region of IGSCC located by SEM fractography
- The sample was sectioned to allow the oxide layer in the IGSCC region to be examined using the analytical techniques of scanning electron microscopy with energy dispersive x-ray analysis, laser raman microprobe spectroscopy and secondary ion mass spectroscopy.
- SEM examination confirmed that the oxide layer had been retained on the surface of the sample. Cracks which appeared to follow grain boundaries were observed penetrating the sample in the IGSCC region. The cracks also contained oxide.
- The oxide on the surface of the sample and in the larger cracks was of a duplex character. The oxide adjacent to the metal was chromium rich and the layer remote from the metal was predominantly composed of iron and oxygen.
- EDX linescans taken across the oxide within a crack indicated that the iron rich oxide also contained sulphur, no sulphur was detected within the oxide on the surface of the sample.
- The same area of the sample was examined using LRM. The main corrosion product detected on the surface and within cracks was Fe_3O_4. Within the duplex scale areas, the oxide was deficient in iron. No evidence was found for the presence of chromia or sulphate. However the features on the sample, particularly in the crack were at the spatial resolution limit of the technique.
- The same area of the sample was also examined using SIMS. Again evidence was found of a duplex oxide with a chromium rich oxide adjacent to the metal and an iron rich oxide away from the metal. As with the LRM no evidence of sulphur was found.

Conclusions

All three analytical techniques were used to examine the same area of IGSCC on a CT specimen. Each technique was capable of detecting the presence of a duplex scale which was chromium rich adjacent to the metal and iron rich beyond.

Sulphur was detected associated with the iron rich oxide using the SEM but no evidence of sulphur was found using either LRM or SIMS.

The present work has demonstrated the capability of SEM-EDX in the analysis of this type of sample. The advantage of EDX over SIMS in the detection of sulphur may lie in the fact that the volume of material analysed with EDX extends to a depth of approximately 1• m and thus contains many more sulphur atoms than are found in the few atomic layers analysed by SIMS.

Figures

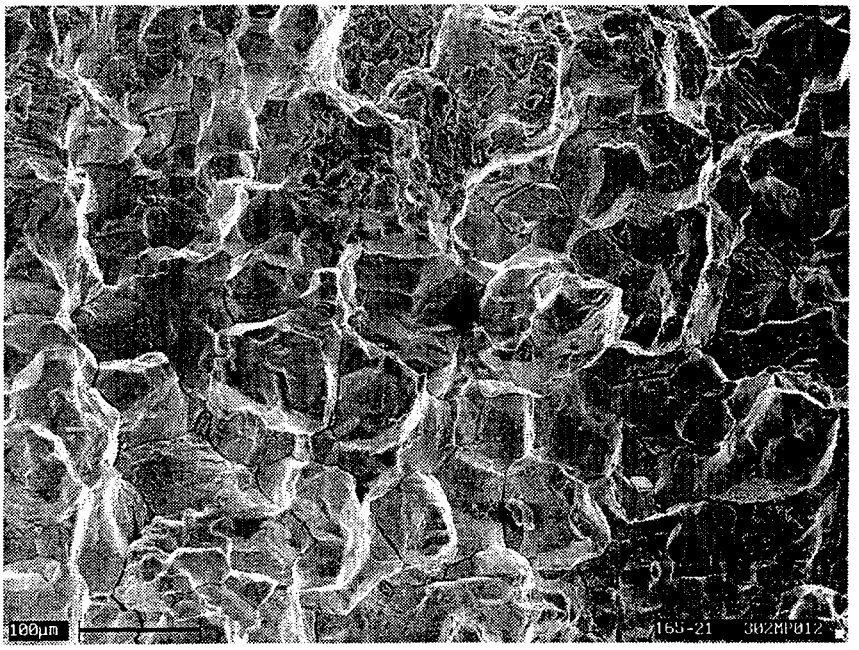

Figure 1: *SEM secondary electron image of IGSCC region*

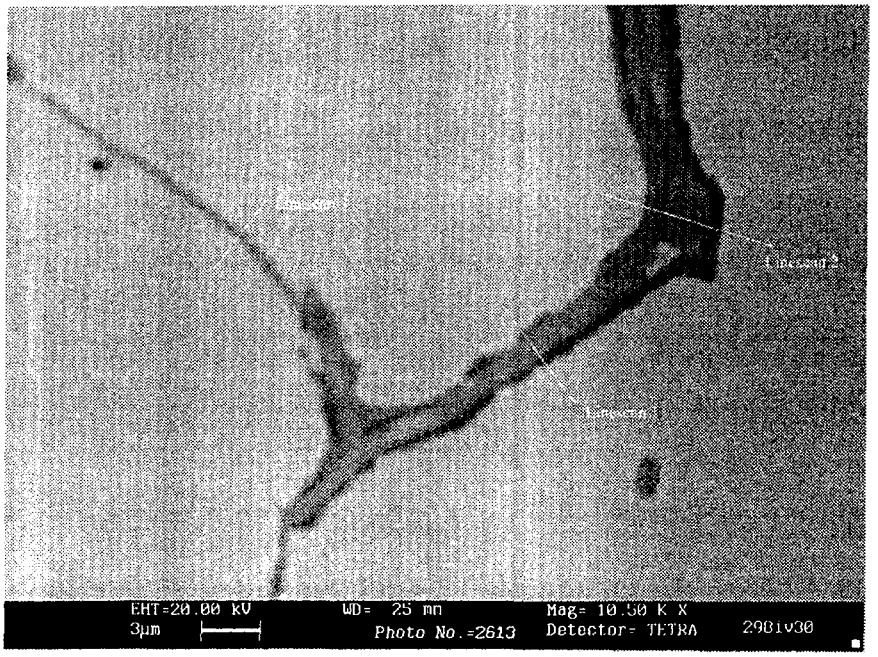

Figure 2: *SEM backscattered electron image of duplex oxide scale within a crack showing position of linescans 1, 2 and 3*

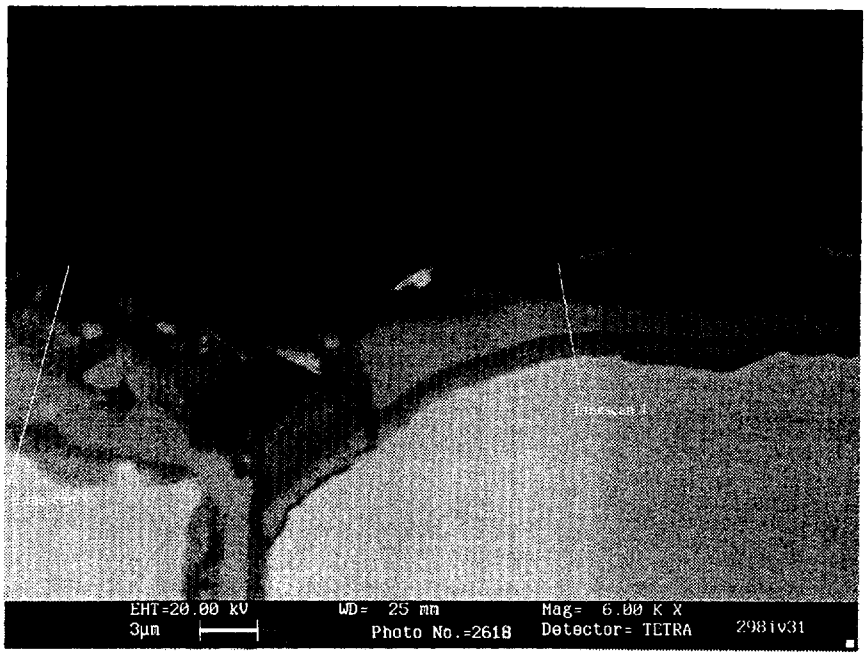

Figure 3: *SEM backscattered electron image of duplex oxide scale on sample surface showing position of linescans 4 and 5*

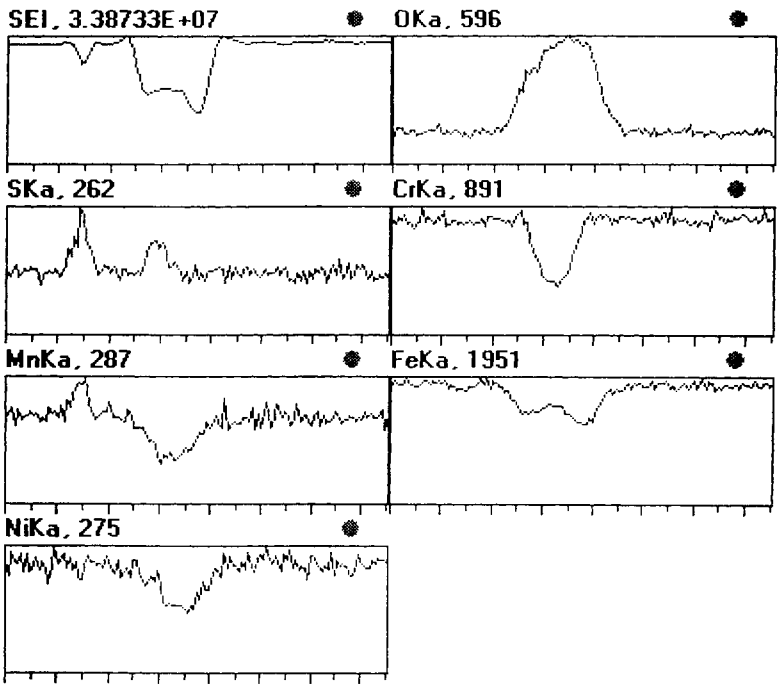

Figure 4: *Linescan 1 across crack*

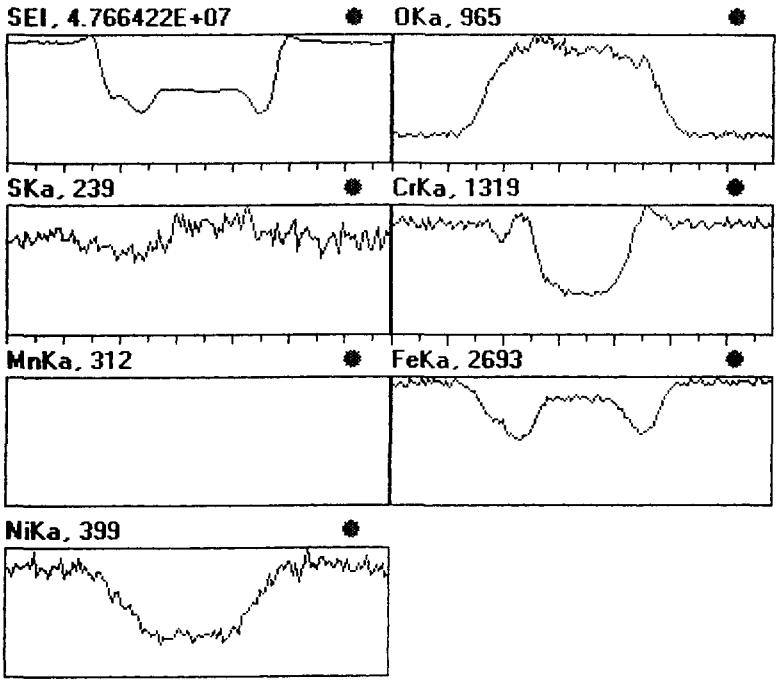

Figure 5: *Linescan 2 across crack*

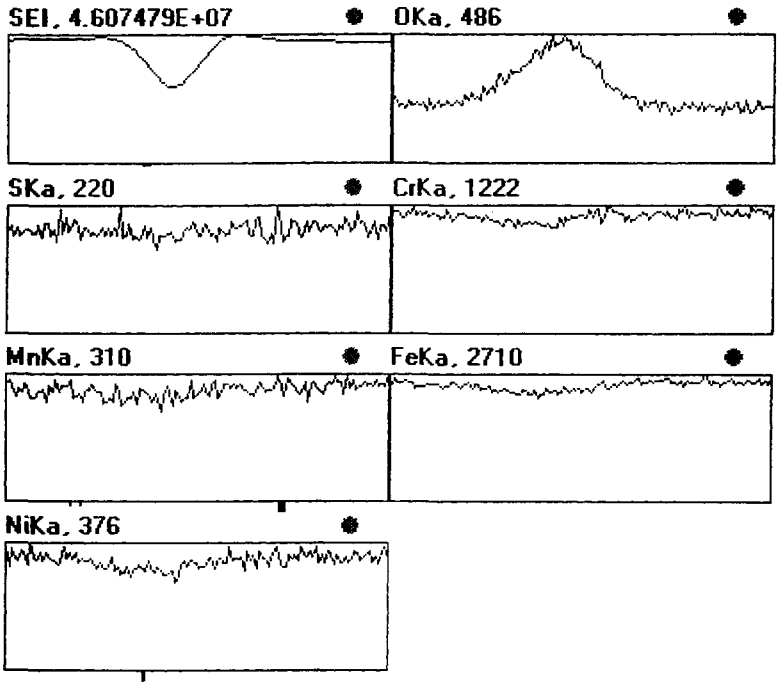

Figure 6: *Linescan 3 across a narrow region of crack*

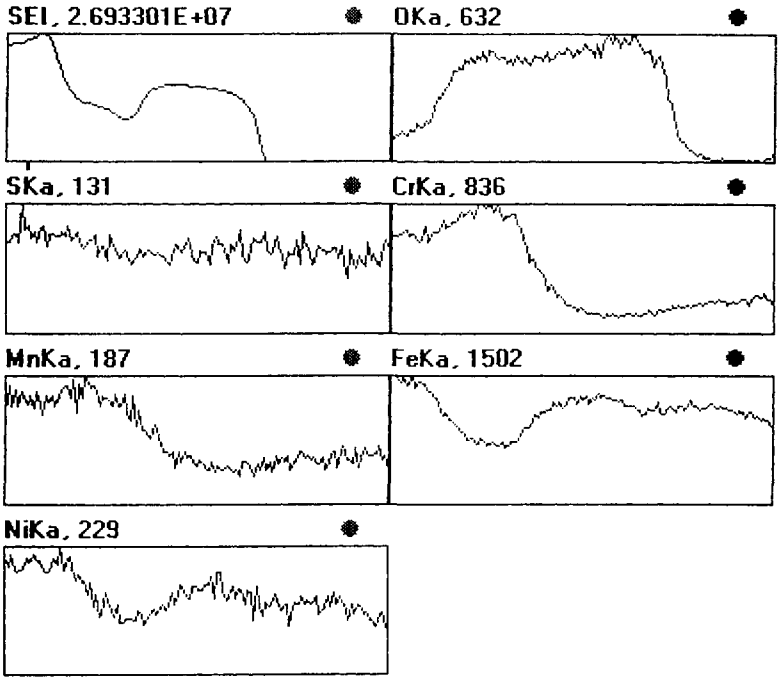

Figure 7: *Linescan 4 across oxide on surface of sample*

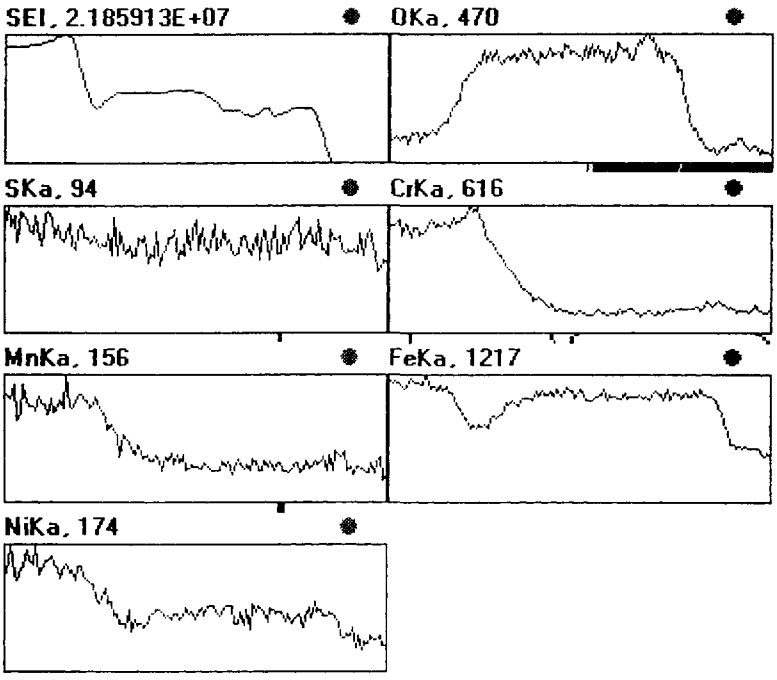

Figure 8: *Linescan 5 across on surface of sample*

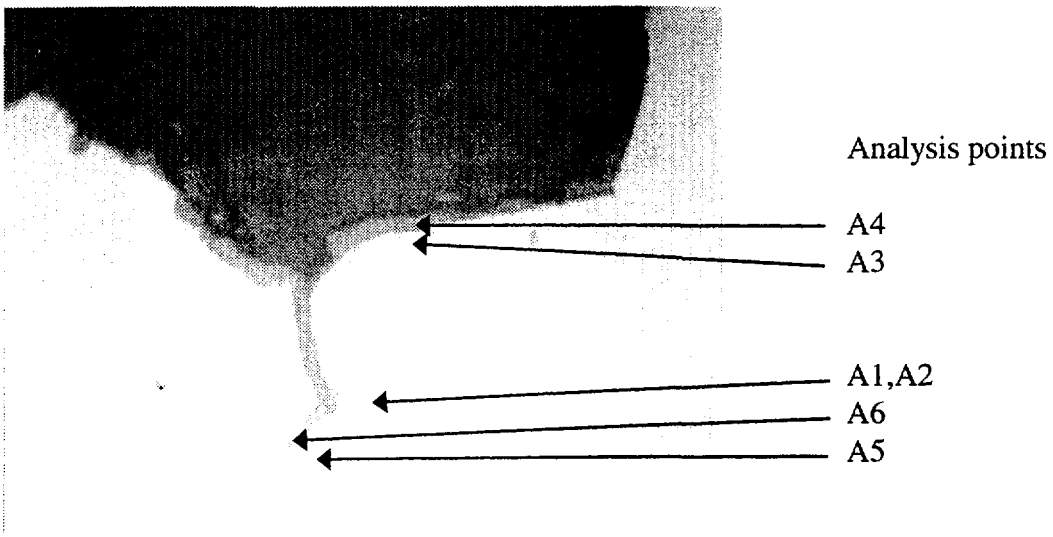

Figure 9: *Optical micrograph (x 800) of the crack previously examined by SEM*

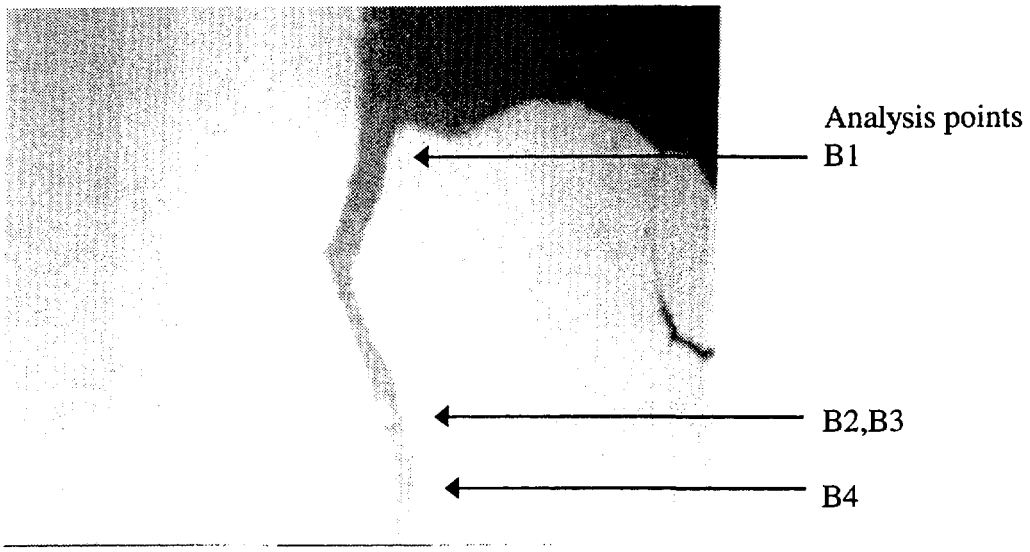

Figure 10: *Optical micrograph (x 800) of the second crack examined by LRM*

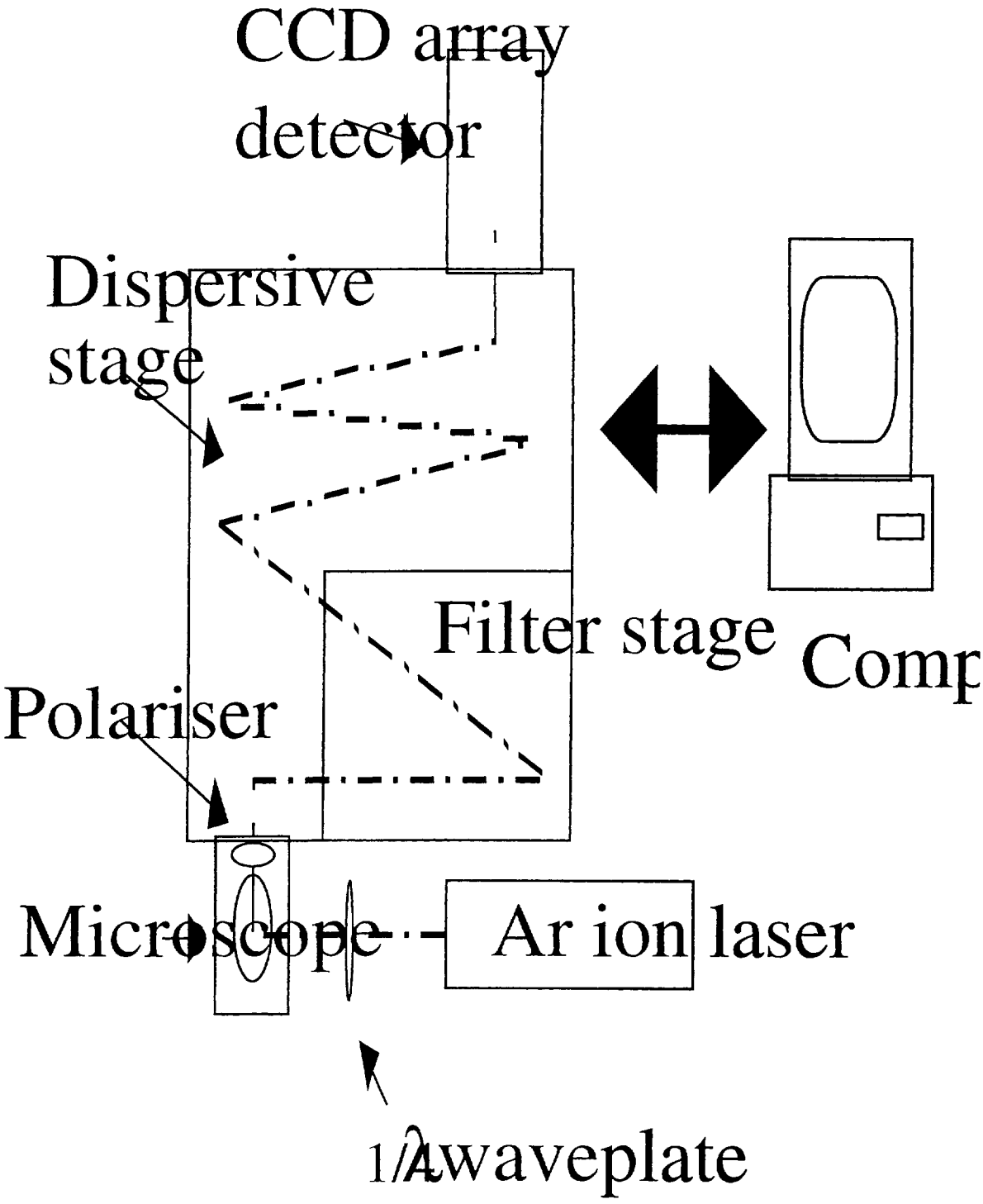
CCD array
detector
Dispersive
stage
Filter stage
Comp
Polariser
Microscope
Ar ion laser
1/4waveplate

Figure 11: *Schematic of Laser Raman Microprobe*

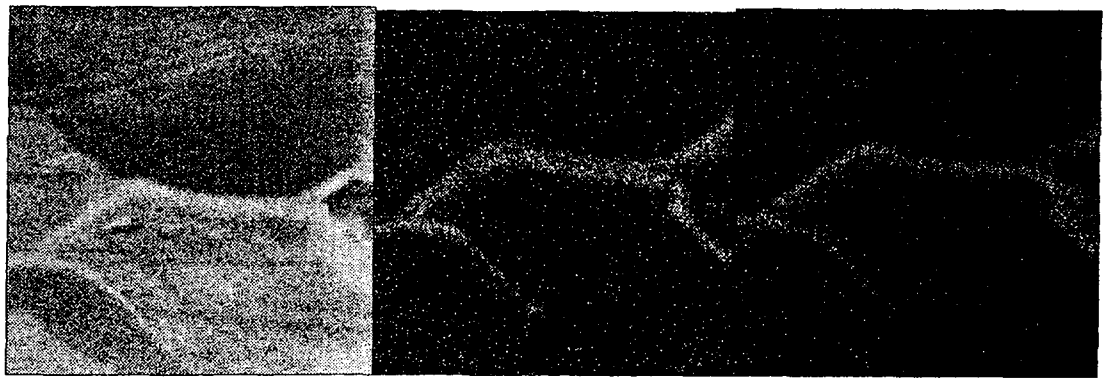

Figure 12: *Secondary electron, chromium and iron images from the SIMS.*

STATENS KÄRNKRAFTINSPEKTION
Swedish Nuclear Power Inspectorate

Postadress/Postal address	Telefon/Telephone	Telefax	Telex
SKI SE-106 58 Stockholm	Nat 08-698 84 00 Int +46 8 698 84 00	Nat 08-661 90 86 Int +46 8 661 90 86	11961 SWEATOM S